ARTICLES
PUBLISHED ONLINE: 6 FEBRUARY 2017 | DOI: 10.1038/NPHYS4028
nature physics

Emergent Dirac fermions and broken symmetries in confined and deconfined phases of Z_2 gauge theories

Snir Gazit[1]*, Mohit Randeria[2] and Ashvin Vishwanath[1,3]

Lattice gauge theories are used to describe a wide range of phenomena from quark confinement to quantum materials. At finite fermion density, gauge theories are notoriously hard to analyse due to the fermion sign problem. Here, we investigate the Ising gauge theory in 2 + 1 dimensions, a problem of great interest in condensed matter, and show that it is free of the sign problem at arbitrary fermion density. At generic filling, we find that gauge fluctuations mediate pairing, leading to a transition between a deconfined BCS state and a confined BEC. At half-filling, a π-flux phase is generated spontaneously with emergent Dirac fermions. The deconfined Dirac phase, with a vanishing Fermi surface volume, is a non-trivial example of violation of Luttinger's theorem due to fractionalization. At strong coupling, we find a single continuous transition between the deconfined Dirac phase and the confined BEC, in contrast to the expected split transition.

In recent years, gauge theories have become increasingly important in condensed matter physics. In contrast to high-energy physics, where the lattice gauge theory is an approach to regularize QCD and analyse confinement[1], gauge fields are emergent in condensed matter, and lattice gauge theories are effective low-energy theories. Important examples include boson-vortex duality[2–4], quantum spin liquids[5–8], quantum dimer models[9,10] and frustrated magnetism[11–13]. In addition, methods for engineering lattice gauge theories in cold atomic systems have been recently proposed[14].

The simplest, and historically the first, example is the Ising lattice gauge theory (ILGT) with a discrete $\mathbb{Z}_2$ local symmetry. It was introduced[15] as a statistical mechanics model that exhibits a phase transition without any symmetry breaking. The 2 + 1-dimensional (2 + 1)D ILGT undergoes a $T = 0$ confinement/deconfinement phase transition that is in the 3D classical Ising model universality class. This can be seen easily by establishing a duality between the (2 + 1)D ILGT and the 2D transverse field Ising model[1]. The deconfined phase of the IGLT is of great interest in condensed matter physics, since it is one of the simplest examples of a state with topological order which exhibits long-range entanglement despite exponentially decaying correlations, and ground state degeneracy on manifolds with non-trivial topology[16–18].

Coupling to dynamical matter fields can have a dramatic effect on the phase diagram of pure gauge theories. Some notable examples are the smooth evolution between the confining and Higgs phases of lattice gauge theories[19], an emergent deconfined phase in compact QED3[20,21], a theory known to be confining in the absence of matter fields, and the loss of asymptotic freedom in (3 + 1)D QCD with a sufficiently large number of flavours of fermions.

In this paper we address the fundamental question of elucidating the phases and phase transitions of dynamical fermions coupled to a $\mathbb{Z}_2$ lattice gauge theory in (2 + 1) dimensions. Analytical approaches for lattice gauge theories are useful only at strong and weak coupling, and Quantum Monte Carlo (QMC) simulations are the only known way to bridge the gap between these limits. However, with a finite density of fermions, QMC simulations are usually plagued by the sign problem. Integrating out the fermions in the imaginary time functional integral leads in general to an effective action with a fluctuating sign, or even worse, one that is complex, and leads to uncontrolled statistical errors in the QMC.

For fermions coupled to IGLT, however, we introduce a sign-problem-free QMC algorithm at arbitrary chemical potential μ, provided there are an even number of fermion flavours—for example, spin ↑ and ↓. The absence of a sign problem allows us to work on large lattices at low temperature and obtain unbiased results that are numerically exact up to statistical errors.

Our four main results are as follows. We find that the phase diagrams are qualitatively different for $\mu \neq 0$ versus $\mu = 0$, which corresponds to half-filling on the square lattice with nearest-neighbour hopping.

First, for generic filling, the $\mathbb{Z}_2$ gauge fields mediate an attractive interaction between fermions, which are then gapped due to pairing and form a s-wave superconducting (SC) ground state. The superfluids deep in the deconfined phase and deep in the confined phase are reminiscent of BCS pairing and BEC, respectively. However, the BCS superfluid involves deconfined $\mathbb{Z}_2$ gauge fields and is an exotic superfluid, SF* (ref. 8), while the BEC is a conventional superfluid. Thus the evolution from one limit to another cannot be via the usual BCS to BEC crossover[22], and must exhibit a $T = 0$ quantum phase transition at which the gauge fields undergo confinement, similar to the pure IGLT without fermions; see Fig. 1.

Second, precisely at half-filling, we find a new deconfined phase with emergent Dirac excitations. We emphasize that we start with non-relativistic fermions on a square lattice with nearest-neighbour hopping t. But, when t is much larger than the ILGT coupling constant, we find a spontaneously generated π-flux in every plaquette, which then leads to a Dirac excitation spectrum. As explained below, due to particle–hole (PH) symmetry, the SC order is degenerate with charge density wave (CDW) order and under a suitable transformation it maps to antiferromagnetic (AF) order in the 'odd' sector of the ILGT; see Fig. 2.

[1]Department of Physics, University of California, Berkeley, California 94720, USA. [2]Department of Physics, The Ohio State University, Columbus, Ohio 43210, USA. [3]Department of Physics, Harvard University, Cambridge, Massachusetts 02138, USA. *e-mail: snirgaz@berkeley.edu

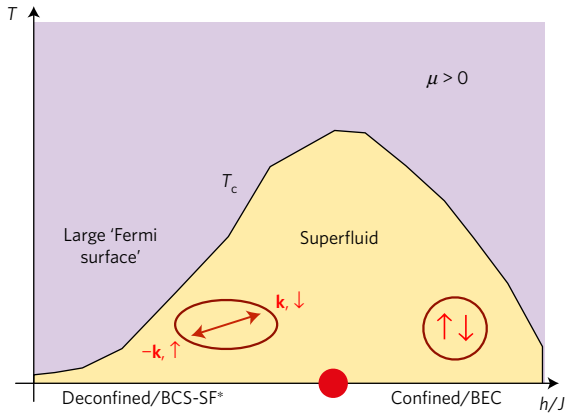

Figure 1 | Schematic phase diagram at fixed $\mu > 0$ as a function of h/J and the temperature T for the 'even' sector of the $\mathbb{Z}_2$ gauge theory. There is a $T = 0$ quantum critical point separating the deconfined BCS superfluid (BCS-SF*) from the confined BEC.

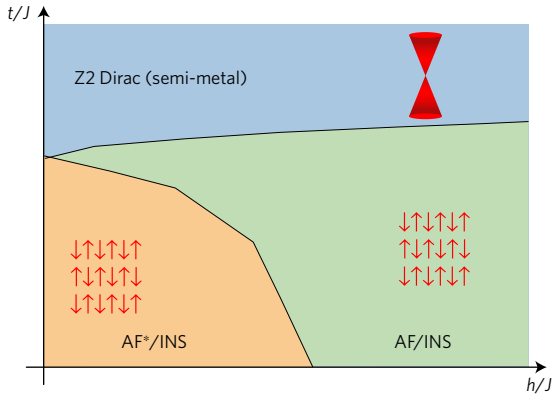

Figure 2 | Schematic $T = 0$ phase diagram at half-filling $\mu = 0$, with a novel, deconfined Dirac semi-metal at large fermion hopping t. In the 'odd' sector of the $\mathbb{Z}_2$ gauge theory the broken-symmetry insulating states are a deconfined antiferromagnet (AF*) and a confined AF. The corresponding phases in the 'even' sector are deconfined BCS/CDW and confined BEC/CDW, respectively.

Third, conventional wisdom holds that the evolution from the deconfined Dirac state to the confined, broken-symmetry phase would proceed through a split transition, wherein first the fermions would acquire a mass gap due to 'chiral symmetry breaking' (via a Gross–Neveu transition[23]), followed by a confinement transition in the usual Ising universality class. Instead, our numerics indicate a very surprising single, continuous transition where symmetry breaking and confinement occur simultaneously. The theoretical description of such a direct transition is an interesting open problem.

Last, at $\mu = 0$, in the extreme weak coupling limit (non-interacting limit of the deconfined BCS phase), the system shows a transition from a large (half-filled) Fermi surface to a deconfined Dirac phase with point nodes. This serves a non-trivial example of a change in Fermi surface area without a broken translational symmetry that arises from the interactions of the fermions with gauge degrees of freedom. Refs 24–26 have suggested that related models and phenomenology may be relevant to the study of strongly correlated electronic systems, such as cuprates and heavy fermions, where Fermi volume changes appear to play an important role.

Model

We consider $\mathcal{H} = \mathcal{H}_{\mathbb{Z}_2} + \mathcal{H}_f$, the Hamiltonian[8] for the ILGT coupled to fermions. The gauge degrees of freedom are Pauli matrices $\sigma^z_{r,\eta}$ and $\sigma^x_{r,\eta}$ on the bonds $b = (\mathbf{r}, \boldsymbol{\eta})$ of a square lattice, with site label $\mathbf{r}$ and $\boldsymbol{\eta} = \hat{\mathbf{e}}_x, \hat{\mathbf{e}}_y$. Their dynamics are governed by

$$H_{\mathbb{Z}_2} = -J \sum_{\mathbf{r}} \prod_{b \in \square_{\mathbf{r}}} \sigma^z_b - h \sum_{\mathbf{r},\boldsymbol{\eta}} \sigma^x_{\mathbf{r},\boldsymbol{\eta}} \quad (1)$$

where $\square_{\mathbf{r}}$, is an elementary plaquette. The fermions hop between nearest neighbour sites and are minimally coupled to the gauge field

$$\mathcal{H}_f = -t \sum_{\mathbf{r},\boldsymbol{\eta},\alpha} \sigma^z_{\mathbf{r},\boldsymbol{\eta}} c^\dagger_{\mathbf{r},\alpha} c_{\mathbf{r}+\boldsymbol{\eta},\alpha} + \text{h.c.} - \mu \sum_{\mathbf{r},\alpha} c^\dagger_{\mathbf{r},\alpha} c_{\mathbf{r},\alpha} \quad (2)$$

Here $c^\dagger_{\mathbf{r},\alpha}$ is the fermion creation operator at site $\mathbf{r}$ with spin $\alpha = \uparrow$ or $\downarrow$, t is the hopping amplitude and μ the chemical potential. J, h and t are all positive.

We must restrict the Hilbert space to include only physical (gauge-invariant) states that obey the Gauss law

$$\prod_{b \in +_{\mathbf{r}}} \sigma^x_b = (-1)^{n^f_{\mathbf{r}}} Q \quad (3)$$

This is a local constraint on the electric fields on the set of bonds $+_{\mathbf{r}}$ emanating from site $\mathbf{r}$. $n^f_{\mathbf{r}} = \sum_\alpha c^\dagger_{\mathbf{r},\alpha} c_{\mathbf{r},\alpha}$ is the fermion number operator and Q defines the even/odd sectors of the ILGT. $Q = 1$ in the 'even' sector, with no $\mathbb{Z}_2$ background charge, whereas $Q = -1$ in the 'odd' sector with one $\mathbb{Z}_2$ charge per unit cell[8,27].

The constraint (3) is imposed exactly via a temporal Ising gauge field, as shown in the Methods. We then integrate out the fermions and show that in the 'even' sector ($Q = 1$) there is no sign problem at any density, and the partition function can be sampled using QMC techniques. For the 'odd' sector ($Q = -1$) sign-problem-free QMC is only possible at half-filling.

In addition, we face the problem of fermion zero modes at half-filling, where configurations with a vanishing weight $\det G^{-1}$ make a finite contribution $G \det G^{-1}$ to observables. We show in the Supplementary Methods how we solve this problem in our numerical simulations.

Symmetries

The global symmetries of our $\mathbb{Z}_2$ gauge theory play a crucial role in our analysis. The fermions c_α carry a $SU(2)_s$ spin and a global $U(1)$ charge, in addition to their $\mathbb{Z}_2$ gauge charge.

At half-filling, $\mu = 0$, both $\mathcal{H}$ and the constraint are invariant under a PH transformation $c_{\mathbf{r},\alpha} \to (-1)^r c^\dagger_{\mathbf{r},\alpha}$ for both spins. The symmetry is enlarged to a $SU(2)_s \times SU(2)_p$, where $SU(2)_p$ is a pseudospin symmetry just as in the Hubbard model[28], under which SC pairing is rotated into CDW order. PH transforming only one spin species leaves $\mathcal{H}$ invariant but changes the sign of Q in (3), thus generating an exact mapping between the even and odd sectors at $\mu = 0$. This maps the SC/CDW order in the even sector to AF order in the odd sector, analogous to the Hubbard model[29].

Translations T_x, T_y allow us to define a unit cell and, in conjunction with the conserved $U(1)$ charge, a filling. However, since the fermions c are not gauge invariant, translational symmetry can be implemented projectively[30]. For our $\mathbb{Z}_2$ gauge theory, the two translation generators of the square lattice acting on the fermions must either commute or anticommute: $T_x T_y = \pm T_y T_x$. Physically, the two possibilities correspond to the zero and π flux phases, respectively, as discussed below.

Confinement and BCS–BEC crossover

Let us look at the even sector at a generic filling $\mu > 0$. (The $\mu < 0$ case is related by a PH transformation.) We first describe the physical picture in various limits and then turn to QMC results, Deep in the confining phase $h \gg J$ and $h \gg t$, the electric field (σ^x) term dominates, and the ground state has $\sigma^x_{\mathbf{r},\boldsymbol{\eta}} = 1$ on every bond. The fermions form on-site $|\uparrow\downarrow\rangle$ pairs (tightly confined

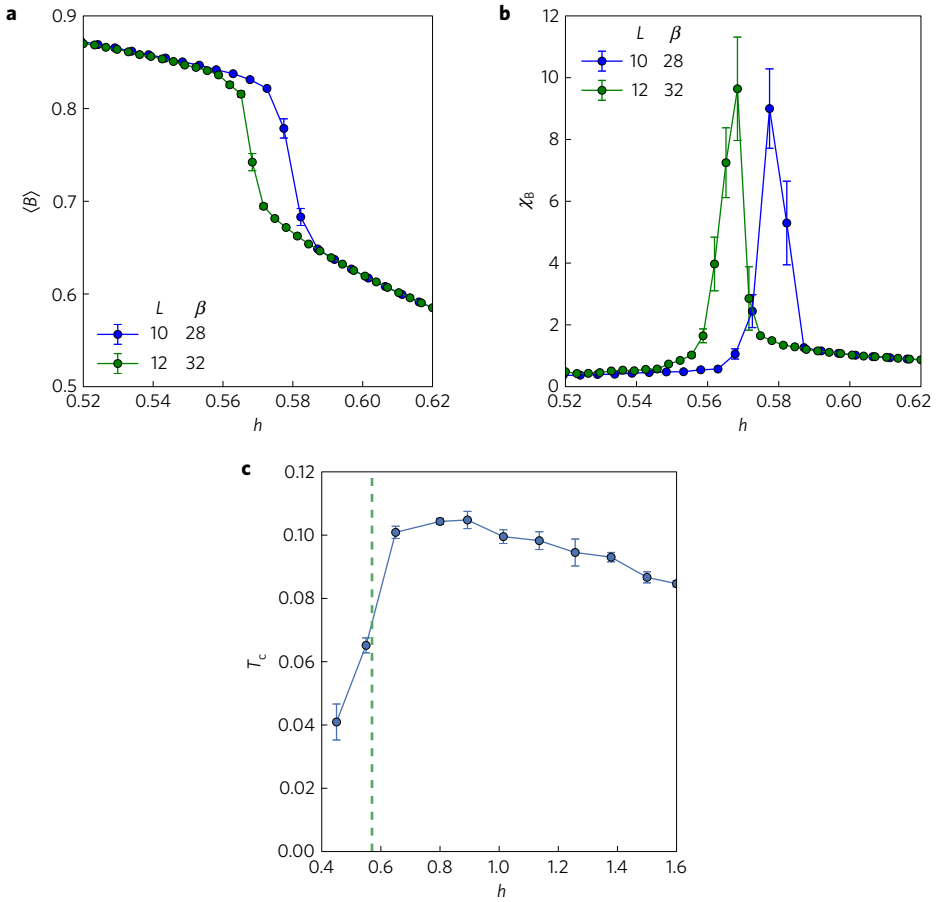

Figure 3 | QMC results for confinement and superconductivity as a function of h at $J=1$, $t=0.5$, $\mu=0.3$ on $L \times L$ lattices at temperature $T=1/\beta$. The error bars are statistical and correspond to one standard deviation. **a**, The average $\mathbb{Z}_2$ magnetic flux $\langle B\rangle$ drops from unity deep in the deconfined phase at small h to zero deep in the confined phase at large h. **b**, Magnetic flux susceptibility χ_B shows a peak at the confinement transition. **c**, Variation of T_c across the confinement transition estimated from the superfluid density for $L=10$. The dashed line is the critical h_c estimated from the peak in χ_B ($L=12, \beta=32$) in **b**.

bosonic molecules) to minimize the electric field cost necessary to satisfy the constraint (3). Quantum corrections lead to an effective hopping $\sim t^2/h$ for these hard-core bosons. The ground state in the confined limit is thus a BEC.

Next we consider the limit $h \ll J$, deep in the deconfined phase. The magnetic term in $\mathcal{H}$ dominates and the gauge-invariant ground state is the zero flux state with $\prod_{\square} \sigma^z = 1$ in every plaquette. Choosing the axial gauge (on an infinite lattice) we can write this as $\sigma^z = 1$ on each bond. The fermions then decouple from the gauge fields, and their $h=0$ ground state is the Fermi sea obtained by filling the square lattice cosine band up to μ. For small h/J we expect[1] that the $\mathbb{Z}_2$ gauge fields meditate a weak, short-range attractive interaction between the fermions, leading to a Cooper instability of the Fermi surface and a BCS-like ground state. At $T=0$, this state is actually a fractionalized superfluid, dubbed SF* (ref. 8), with gapped vison excitations and ground state degeneracy on a cylinder or torus.

The fermions are gapped by pairing in both phases, and as a result we expect that the confinement transition is in the same universality class as the pure $\mathbb{Z}_2$ gauge theory in $(2+1)$D, which is dual to the transverse field Ising model. The transition is, however, distinct from the usual smooth BCS–BEC crossover, since confinement involves a $T=0$ quantum phase transition.

We next present QMC results as a function of h at fixed $J=1$, $t=0.5$ and $\mu=0.3$. In Fig. 3a we plot the average $\mathbb{Z}_2$ magnetic flux $\langle B\rangle$. (See Methods for the precise definition of this and other observables). For small h, we find, as expected, a zero flux state with $\langle B\rangle \to 1$ in the deconfined phase. With increasing h, the $\mathbb{Z}_2$ flux decreases monotonically towards the confining phase. The critical fluctuations are probed using the $\mathbb{Z}_2$ flux susceptibility χ_B in Fig. 3b, which develops a peak at $h_c = 0.56(2)$ that marks the confinement transition.

We compute the superfluid stiffness ρ_s to demonstrate that the fermions are in a SC state, locating the 2D transition temperature T_c using the universal jump $\rho_s(T_c^-) = 2T_c/\pi$ in Berezinskii–Kosterlitz–Thouless (BKT) theory[31]. We see from Fig. 3c that T_c remains finite across the confinement transition at h_c (marked with a dashed vertical line estimated from χ_B). $T_c(h)$ has a non-monotonic variation, with a maximum that seems to be above the confinement h_c and a sharp drop in T_c on the deconfined side just below h_c.

Half-filling

In the rest of the paper, we focus on half-filling, where the enhanced symmetry leads to the phase diagram in Fig. 2. Recall that the single-spin PH transformation at $\mu=0$ maps the even sector of the ILGT to the odd sector, thus all the results can be interpreted appropriately in either sector.

In the weak hopping limit $t \ll J$, the deconfined BCS to confined BEC evolution with h/J is similar to the $\mu \neq 0$ case, with one crucial difference. The $SU(2)_p$ pseudospin symmetry at $\mu=0$ leads to a degeneracy between SC and CDW order in the even sector, and thus $T_c=0$ (unlike the BKT transition for $\mu \neq 0$). The even-odd sector transformation maps SC/CDW to AF order, for which the $SU(2)$ symmetry is obvious.

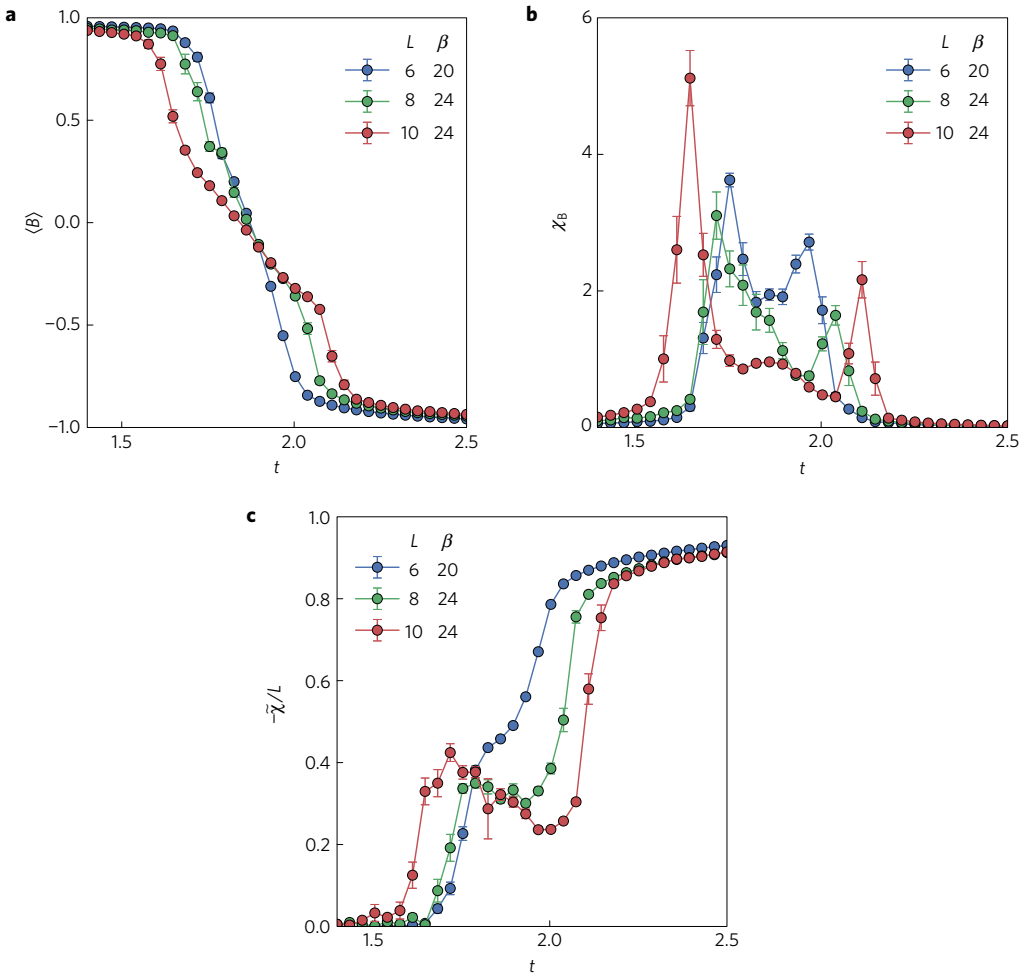

Figure 4 | The evolution from a deconfined BCS state to a deconfined Dirac phase with increasing t in the weak coupling regime $J = 0.3$ $h = 0.1$. The error bars are statistical and correspond to one standard deviation. **a**, The average Ising magnetic flux, $\langle B \rangle$, goes from +1 (or zero flux) deep in the deconfined BCS phase at small t to −1 (or π-flux) deep in the deconfined Dirac limit at large t. **b**, The Ising magnetic flux susceptibility χ_B exhibits two peaks as a function of t, indicating two distinct confinement transitions, with an intermediate-t phase which is a confined BEC. **c** Scaled orbital (diamagnetic) susceptibility $-\tilde{\chi}/L$ (see text) as a function of t. This goes to unity independently of L in the Dirac phase at large t.

Emergent Dirac excitations

The situation is qualitatively different in the $t \gg J$ limit, where determining the ground state amounts to finding the gauge field configuration that minimizes the fermion kinetic energy. At half-filling, the result is a uniform π-flux phase[7,32], with $\prod_{\square} \sigma^z = -1$ in every plaquette, which leads to an excitation spectrum with two Dirac nodes.

This is simplest to see in the $h = 0$ limit, where ILGT quantum fluctuations are absent and by assuming a uniform flux configuration we can analytically find the transition from a deconfined 0-flux state, with a large Fermi surface, to the deconfined π-flux Dirac phase. The gain in the fermion kinetic energy (per site) in the π-flux phase is $\Delta E_k = E_k(0) - E_k(\pi) = 0.295\,t$, while the energy loss for the Ising sector is $\Delta E_J = -2J$. Comparing the two, we obtain a first-order transition (level crossing) at $t/J = 6.77$.

We emphasize that the π-flux phase does not lead to a doubling of the unit cell. It arises from the projective realization of translational symmetry: $T_x T_y = -T_y T_x$. The change in the Fermi surface (FS) area from a large (half-filled) FS to Dirac nodes, without any translational symmetry breaking, seems to violate Luttinger's theorem. But, in a deconfined phase, the Oshikawa flux insertion argument permits this change in FS area by a density corresponding to half-filling.

$\mu = 0$ Phase diagram

Next we look at the effect of gauge fluctuations at non-zero h/J on the two deconfined phases. The 0-flux phase with a FS is unstable to symmetry breaking at arbitrarily small h. However, the vanishing density of states makes the π-flux Dirac state stable against weak perturbations. At finite h/J we find numerical evidence for an intermediate (confined) phase between the deconfined BCS/CDW and Dirac states.

In Fig. 4a, we show QMC results for the $\mathbb{Z}_2$ magnetic flux $\langle B \rangle$ as a function of t for $J = 0.3, h = 0.1$. It decreases monotonically from the $\langle B \rangle = 1$ or 0-flux state at small t to $\langle B \rangle = -1$ at large t, characteristic of a deconfined phase with a spontaneously generated π-flux per plaquette.

We see from Fig. 4b that the $\mathbb{Z}_2$ flux susceptibility χ_B shows two peaks as a function of t, indicating two distinct phase transitions. From the general topology of the phase diagram, including the large h/J results described below, we identify the intermediate phase lying between the deconfined BCS/CDW and deconfined Dirac phases as a confined BEC/CDW. An intuitive way to understand this is as follows. Upon increasing the fermion kinetic energy one reduces the effective $\tilde{J}$ which controls the plaquette term in the ILGT, thus leading to confinement. For sufficiently large t, it is reduced so much that effectively $\tilde{J} < 0$, leading to the π-flux phase. We did not find evidence for flux lattice states that break

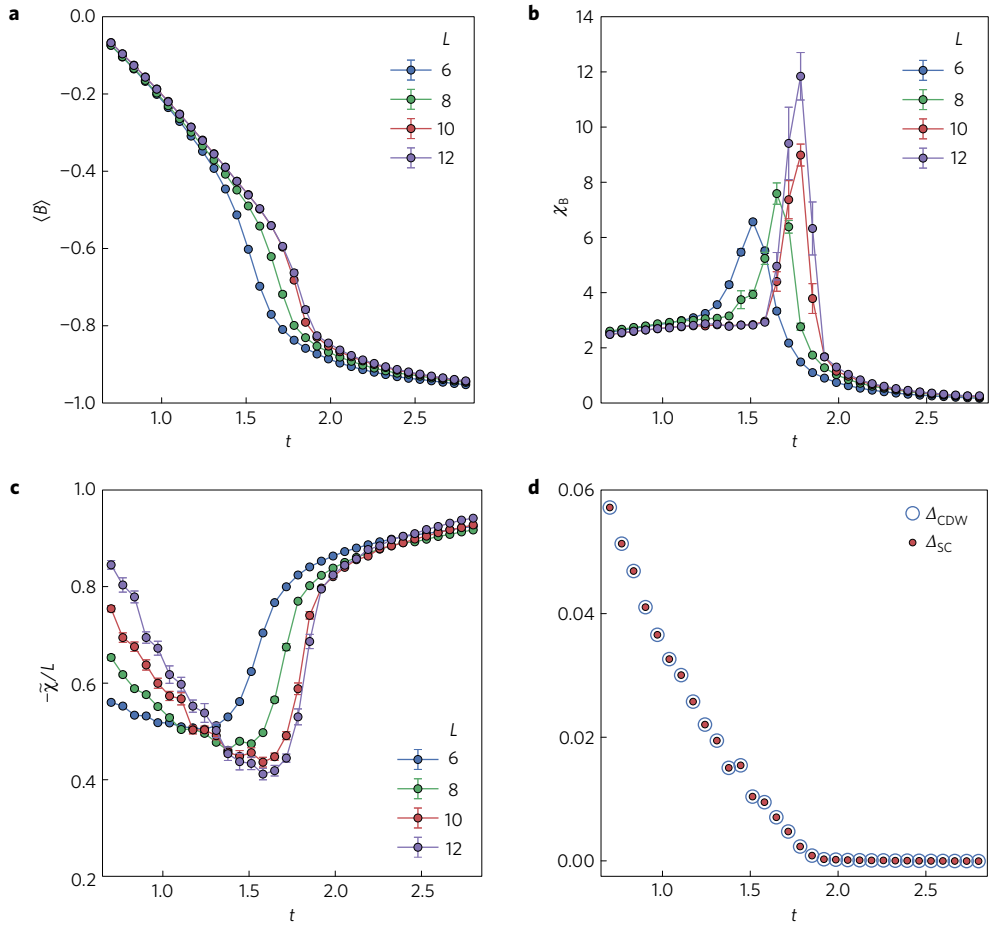

Figure 5 | Phase transition from a confined BEC to a deconfined Dirac phase driven by increasing t at $\mu = 0$ with $J = 0.1, h = 0.2$. The error bars are statistical and correspond to one standard deviation. **a**, The average Ising flux, $\langle B \rangle$, goes from 0 deep in the confined phase to -1 ('π-flux') deep in the deconfined limit. **b**, The Ising flux susceptibility, χ_B, whose singularity, at $t_c = 1.8(1)$, indicates the confinement transition. **c**, Scaled magnetic susceptibility $-\widetilde{\chi}/L$, goes to unity independently of L in the Dirac phase at large t; see text. **d**, S-wave pairing, Δ_{SC} and CWD , Δ_{CDW} order parameters extrapolated to $T = 0$ and then to the thermodynamic limit. Both quantities are finite and equal (as required by symmetry) in the confined phase and vanish continuously at $t_c = 1.8(1)$.

translational symmetry. Finite size effects may frustrate such configurations, and thus determining the thermodynamic ground state may require investigation of large lattices beyond the reach of our current numerics.

Probing the Dirac excitations in the π-flux phase is challenging, since the fermion Green's function is not gauge invariant. We therefore turn to the static orbital susceptibility $\chi(q)$, which for free Dirac fermions is $\chi_{\mathrm{Dirac}}(\mathbf{q}) = -g_s g_v v_F/16q$ in the small-q limit[33,34]. Here, $g_s = 2$ ($g_v = 2$) are the spin (valley) degeneracies and v_F the Fermi velocity. It is convenient to define $-\widetilde{\chi}/L \equiv -4\pi\chi_{\mathrm{Dirac}}(q = 2\pi/L)/Lt = v_F/2t$, a dimensionless observable normalized so that it is unity in the non-interacting π-flux phase with $v_F = 2t$ at the Dirac nodes. We plot QMC results for the scaled orbital susceptibility in Fig. 4c and see that $(-\widetilde{\chi}/L) \to 1$ at large t, independently of L, which is direct evidence for Dirac nodes.

Confinement and symmetry breaking

We finally turn to the phase diagram as a function of hopping t at strong coupling (large h/J). At small t/J we expect a confined, broken-symmetry (BEC/CDW) state, and a deconfined Dirac phase at large t/J. We show that this is borne out in the QMC data but, most surprisingly, we find a single continuous transition with the onset of both confinement and symmetry breaking.

In Fig. 5a, we show QMC results at $h = 0.2$ and $J = 0.1$. The $\mathbb{Z}_2$ flux $\langle B \rangle$ (t) decreases monotonically, going from $\langle B \rangle = 0$, deep in the confined phase at small t, to $\langle B \rangle = -1$ in the π-flux phase at large t. From Fig. 5b we see that the $\mathbb{Z}_2$ flux susceptibility χ_B has a peak that increases with system size, and signals the confinement (small t) to deconfinement (large t) transition at $t_c = 1.8(1)$.

We again use the scaled orbital susceptibility $-\widetilde{\chi}/L$ to characterize the Dirac excitations in the deconfined phase, and see from Fig. 5c that it approaches unity in the large-t limit. To characterize the broken $SU(2)$ pseudospin symmetry in the confined phase, we show in Fig. 5d the s-wave SC and CDW order parameters, Δ_{SC} and Δ_{CDW} respectively. Since $T_c = 0$ here, we first extrapolate the data to $T = 0$ and then take $L \to \infty$. In the confined phase, both order parameters are finite and indeed equal, and they vanish continuously at $t_c = 1.8(1)$ upon approaching the deconfined Dirac phase.

Finite size scaling

Our results suggest an unexpected continuous transition at $\mu = 0$ with the simultaneous occurrence of confinement and symmetry breaking. This transition would thus be in a novel universality class, distinct from either chiral symmetry breaking[23] or confinement in the ILGT. To elucidate its universal critical properties, we find it convenient to use h to tune across the transition, with the choice of plaquette coupling $J = -1$ and hopping amplitude $t = 1$. The negative J leads to π-flux per plaquette and a deconfined Dirac phase at small h, whereas the system is in a confined, broken-symmetry state at large h.

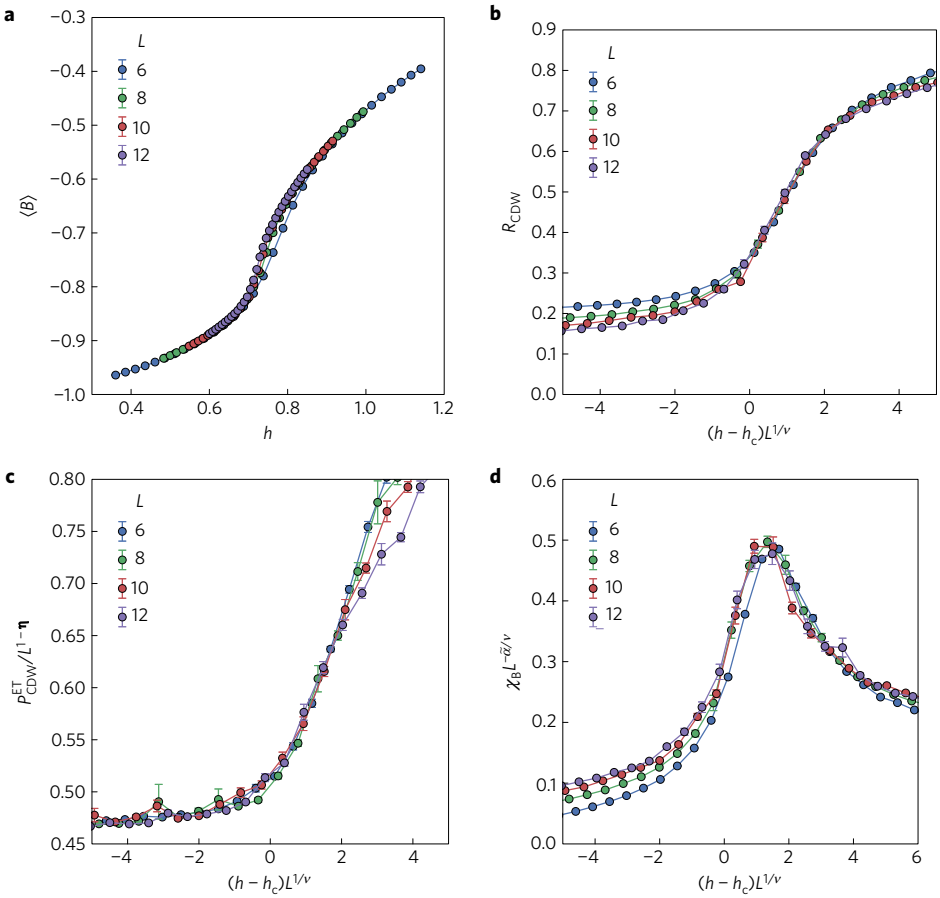

Figure 6 | Finite size scaling analysis of the phase transition between a confined BEC/CDW and a deconfined Dirac phase driven by increasing h at $\mu = 0$ with $J = -1, t = 1.0$. We assume a dynamical exponent $z = 1$ and scale the inverse temperature as $\beta = L$. The error bars are statistical and correspond to one standard deviation. **a**, The average Ising flux evolves from $\langle B\rangle \to -1$ ('π-flux') at small h deep in the Dirac deconfined phase to $\langle B\rangle \to 0$ on increasing h towards the confined, broken-symmetry phase. **b**, Universal scaling function $R_{CDW} = \mathcal{R}(\delta h L^{1/\nu})$ with correlation length exponent $\nu = 0.58(5)$ and critical coupling $h_c = 0.71(2)$. **c**, Universal scaling function of the equal-time CDW susceptibility $P^{ET}_{CDW} = L^{1-\eta}\mathcal{P}(\delta h L^{1/\nu})$ with $\eta = 1.0(3)$. **d**, Universal scaling function of the Ising flux susceptibility, $\chi_B = L^{\tilde{\alpha}/\nu}\mathcal{F}(\delta h L^{1/\nu})$, with $\tilde{\alpha} = 0.25(5)$.

We use finite size scaling with a dynamical critical exponent $z = 1$. We thus scale the inverse temperature linearly with the system size $\beta = L$. In Fig. 6a, we plot the evolution of the Ising flux $\langle B\rangle$ with h, from $\langle B\rangle \to -1$ (π-flux phase) at small h in the Dirac deconfined phase to $\langle B\rangle \to 0$ in the confined phase at large h.

We determine the critical h_c and the correlation length exponent ν from the ratio $R_{CDW} = 1 - P_D(G - 2\pi/L, 0)/P_D(G, 0)$, where $P_D(q, i\omega_m)$ is the density–density correlation at wave vector q and Matsubara frequency ω_m, and $G = (\pi, \pi)$ is the Bragg ordering vector. R_{CDW} is dimensionless and takes a simple scaling form $R_{CDW} = \mathcal{R}(\delta h L^{1/\nu})$ near criticality, with $\delta h = h - h_c$. Indeed, as shown in Fig. 6b, we find data collapse for different system sizes with $\nu = 0.58(5)$ and $h_c = 0.71(2)$.

Next, we determine the anomalous exponent $\boldsymbol{\eta}$ from $P^{ET}_{CDW} = P_D(G, \tau = 0)$, the equal-time CDW susceptibility, which has the universal scaling form $P^{ET}_{CDW} = L^{1-\eta}\mathcal{P}(\delta h L^{1/\nu})$. The data collapse for P^{ET}_{CDW} in Fig. 6c is obtained for $\boldsymbol{\eta} = 1.0(3)$. As a consistency check, we also performed a similar analysis for the static susceptibility, $P_D(q = G, i\omega_m = 0)$, using the above values of $\boldsymbol{\eta}$, ν and h_c, and found good agreement for $L = 10, 12$. Studies of larger system sizes are required for a more accurate computation of $\boldsymbol{\eta}$; however, the large value of $\boldsymbol{\eta}$ is indeed what one might expect at such a transition.

Finally, we also investigate the Ising gauge field sector, by computing the universal scaling function of the Ising flux susceptibility, $\chi_B = L^{\tilde{\alpha}/\nu}\mathcal{F}(\delta h L^{1/\nu})$. Data collapse is obtained for $\tilde{\alpha} = 0.25(5)$ in Fig. 6d. Importantly, we used here the same ν and h_c that were computed using fermion observables. As an additional consistency check, we note that the exponent ν and $\tilde{\alpha}$ are consistent with the hyper-scaling relation, $2 - \tilde{\alpha} = (d + z)\nu$. All of these results clearly suggest a single continuous transition where confinement and symmetry breaking coincide.

Conclusions

We end with some remarks on the methodological progress and open questions. The QMC sign problem is known to plague most fermion models at arbitrary density, with the exception of the attractive Hubbard model[35]. In recent years, sign-problem-free QMC algorithms have been devised for several interesting problems[36–43]. The algorithm introduced here is, to the best of our knowledge, the first one for fermions coupled to gauge theories. Away from half-filling, a sign-problem-free algorithm for the odd sector is not known. This regime is relevant for understanding superconductivity in doped Mott insulators[8].

The deconfined phase with emergent Dirac excitations at half-filling raises several questions. How does the first-order transition from a large Fermi surface to Dirac nodes at $h = 0$ evolve into the continuous transition seen in the numerics at small, finite h/J? What is the field theory that describes the universal behaviour at the transition from the confined, broken-symmetry phase to the deconfined Dirac phase? These issues are all worthy of further investigation.

Note added in proof: After finalizing the results of this paper we became aware of a QMC study of a related model[44] where the Gauss law is not explicitly enforced. Understanding the precise relation between these works is left to the future.

Methods

Methods, including statements of data availability and any associated accession codes and references, are available in the online version of this paper.

Received 5 September 2016; accepted 3 January 2017; published online 6 February 2017

References

1. Kogut, J. B. An introduction to lattice gauge theory and spin systems. *Rev. Mod. Phys.* **51,** 659–713 (1979).
2. Peskin, M. E. Mandelstam-'t Hooft duality in abelian lattice models. *Ann. Phys.* **113,** 122–152 (1978).
3. Dasgupta, C. & Halperin, B. I. Phase transition in a lattice model of superconductivity. *Phys. Rev. Lett.* **47,** 1556–1560 (1981).
4. Fisher, M. P. A. & Lee, D. H. Correspondence between two-dimensional bosons and a bulk superconductor in a magnetic field. *Phys. Rev. B* **39,** 2756–2759 (1989).
5. Baskaran, G. & Anderson, P. W. Gauge theory of high-temperature superconductors and strongly correlated Fermi systems. *Phys. Rev. B* **37,** 580–583 (1988).
6. Read, N. & Sachdev, S. Spin-Peierls, valence-bond solid, and Néel ground states of low-dimensional quantum antiferromagnets. *Phys. Rev. B* **42,** 4568–4589 (1990).
7. Affleck, I. & Marston, J. B. Large-n limit of the Heisenberg–Hubbard model: implications for high-T_c superconductors. *Phys. Rev. B* **37,** 3774–3777 (1988).
8. Senthil, T. & Fisher, M. P. A. Z_2 gauge theory of electron fractionalization in strongly correlated systems. *Phys. Rev. B* **62,** 7850–7881 (2000).
9. Kivelson, S. A., Rokhsar, D. S. & Sethna, J. P. Topology of the resonating valence-bond state: solitons and high-T_c superconductivity. *Phys. Rev. B* **35,** 8865–8868 (1987).
10. Moessner, R., Sondhi, S. L. & Fradkin, E. Short-ranged resonating valence bond physics, quantum dimer models, and Ising gauge theories. *Phys. Rev. B* **65,** 024504 (2001).
11. Balents, L. Spin liquids in frustrated magnets. *Nature* **464,** 199–208 (2010).
12. Read, N. & Sachdev, S. Large-N expansion for frustrated quantum antiferromagnets. *Phys. Rev. Lett.* **66,** 1773–1776 (1991).
13. Jalabert, R. A. & Sachdev, S. Spontaneous alignment of frustrated bonds in an anisotropic, three-dimensional Ising model. *Phys. Rev. B* **44,** 686–690 (1991).
14. Zohar, E., Cirac, J. I. & Reznik, B. Quantum simulations of lattice gauge theories using ultracold atoms in optical lattices. *Rep. Prog. Phys.* **79,** 014401 (2016).
15. Wegner, F. J. Duality in generalized Ising models and phase transitions without local order parameters. *J. Math. Phys.* **12,** 2259–2272 (1971).
16. Wen, X.-G. Quantum orders and symmetric spin liquids. *Phys. Rev. B* **65,** 165113 (2002).
17. Read, N. & Chakraborty, B. Statistics of the excitations of the resonating-valence-bond state. *Phys. Rev. B* **40,** 7133–7140 (1989).
18. Kitaev, A. & Laumann, C. *Exact Methods in Low-dimensional Statistical Physics and Quantum Computing: Lecture Notes of the Les Houches Summer School: Volume 89, July 2008* Vol. 89, 101 (2010).
19. Fradkin, E. & Shenker, S. H. Phase diagrams of lattice gauge theories with Higgs fields. *Phys. Rev. D* **19,** 3682–3697 (1979).
20. Hermele, M. *et al*. Stability of $u(1)$ spin liquids in two dimensions. *Phys. Rev. B* **70,** 214437 (2004).
21. Nogueira, F. S. & Kleinert, H. Quantum electrodynamics in $2+1$ dimensions, confinement, and the stability of $u(1)$ spin liquids. *Phys. Rev. Lett.* **95,** 176406 (2005).
22. Randeria, M. & Taylor, E. Crossover from Bardeen–Cooper–Schrieffer to Bose–Einstein condensation and the unitary Fermi gas. *Ann. Rev. Condens. Matter Phys.* **5,** 209–232 (2014).
23. Herbut, I. F. Interactions and phase transitions on graphene's honeycomb lattice. *Phys. Rev. Lett.* **97,** 146401 (2006).
24. Sachdev, S., Berg, E., Chatterjee, S. & Schattner, Y. Spin density wave order, topological order, and Fermi surface reconstruction. *Phys. Rev. B* **94,** 115147 (2016).
25. Punk, M., Allais, A. & Sachdev, S. Quantum dimer model for the pseudogap metal. *Proc. Natl Acad. Sci. USA* **112,** 9552–9557 (2015).
26. Nandkishore, R., Metlitski, M. A. & Senthil, T. Orthogonal metals: the simplest non-Fermi liquids. *Phys. Rev. B* **86,** 045128 (2012).
27. Moessner, R., Sondhi, S. L. & Fradkin, E. Short-ranged resonating valence bond physics, quantum dimer models, and Ising gauge theories. *Phys. Rev. B* **65,** 024504 (2001).
28. Zhang, S. Pseudospin symmetry and new collective modes of the Hubbard model. *Phys. Rev. Lett.* **65,** 120–122 (1990).
29. Auerbach, A. *Interacting Electrons and Quantum Magnetism* (Springer Science & Business Media, 2012).
30. Wen, X.-G. *Quantum Field Theory of Many-body Systems: From the Origin of Sound to an Origin of Light and Electrons* (Oxford University Press on Demand, 2004).
31. Nelson, D. R. & Kosterlitz, J. M. Universal jump in the superfluid density of two-dimensional superfluids. *Phys. Rev. Lett.* **39,** 1201–1205 (1977).
32. Lieb, E. H. Flux phase of the half-filled band. *Phys. Rev. Lett.* **73,** 2158–2161 (1994).
33. Koshino, M., Arimura, Y. & Ando, T. Magnetic field screening and mirroring in graphene. *Phys. Rev. Lett.* **102,** 177203 (2009).
34. Ludwig, A. W. W., Fisher, M. P. A., Shankar, R. & Grinstein, G. Integer quantum Hall transition: an alternative approach and exact results. *Phys. Rev. B* **50,** 7526–7552 (1994).
35. Hirsch, J. E. Discrete Hubbard–Stratonovich transformation for fermion lattice models. *Phys. Rev. B* **28,** 4059–4061 (1983).
36. Chandrasekharan, S. Fermion bag approach to fermion sign problems. *Eur. Phys. J. A* **49,** 90 (2013).
37. Li, Z.-X., Jiang, Y.-F. & Yao, H. Solving the fermion sign problem in quantum Monte Carlo simulations by Majorana representation. *Phys. Rev. B* **91,** 241117 (2015).
38. Wang, L., Liu, Y.-H., Iazzi, M., Troyer, M. & Harcos, G. Split orthogonal group: a guiding principle for sign-problem-free fermionic simulations. *Phys. Rev. Lett.* **115,** 250601 (2015).
39. Schattner, Y., Lederer, S., Kivelson, S. A. & Berg, E. Ising nematic quantum critical point in a metal: a Monte Carlo study. *Phys. Rev. X* **6,** 031028 (2016).
40. Berg, E., Metlitski, M. A. & Sachdev, S. Sign-problem–free quantum Monte Carlo of the onset of antiferromagnetism in metals. *Science* **338,** 1606–1609 (2012).
41. Schattner, Y., Gerlach, M. H., Trebst, S. & Berg, E. Competing orders in a nearly antiferromagnetic metal. *Phys. Rev. Lett.* **117,** 097002 (2016).
42. Li, Z.-X., Wang, F., Yao, H. & Lee, D.-H. What makes the T_c of monolayer FeSe on $SrTiO_3$ so high: a sign-problem-free quantum Monte Carlo study. *Sci. Bull.* **61,** 925–930 (2016).
43. Dumitrescu, P. T., Serbyn, M., Scalettar, R. T. & Vishwanath, A. Superconductivity and nematic fluctuations in a model of doped FeSe monolayers: determinant quantum Monte Carlo study. *Phys. Rev. B* **94,** 155127 (2016).
44. Assaad, F. F. & Grover, T. Simple fermionic model of deconfined phases and phase transitions. *Phys. Rev. X* **6,** 041049 (2016).
45. Pordes, R. *et al*. The Open Science Grid. *J. Phys.* **78,** 012057 (2007).
46. Sfiligoi, I. *et al*. *2009 WRI World Congress on Computer Science and Information Engineering* Vol. 2, 428–432 (IEEE, 2009).
47. Towns, J. *et al*. XSEDE: accelerating scientific discovery. *Comput. Sci. Eng.* **16,** 62–74 (2014).

Acknowledgements

We thank S. Sachdev and T. Senthil for discussions. S.G. was supported by the Simons Investigators Program, the California Institute of Quantum Emulation and the Templeton Foundation. M.R. acknowledges support from NSF DMR-1410364 and the hospitality of the Berkeley CMT Group in Fall 2015. A.V. acknowledges support from the Templeton Foundation and a Simons Investigator Award. Part of this work was performed at the Aspen Center for Physics, which is supported by National Science Foundation grant PHY-1066293. This research was done using resources provided by the Open Science Grid[45,46], supported by the NSF, and used the Extreme Science and Engineering Discovery Environment[47] (XSEDE), supported by NSF grant ACI-1053575.

Author contributions

S.G. conceived of and carried out the numerical simulations and data analysis. All authors contributed to the development of the theoretical results and to the writing of the manuscript.

Additional information

Supplementary information is available in the online version of the paper. Reprints and permissions information is available online at www.nature.com/reprints. Correspondence and requests for materials should be addressed to S.G.

Competing financial interests

The authors declare no competing financial interests.

Methods

Absence of sign problem in DQMC. The grand canonical partition function $\mathcal{Z}(\beta,\mu)$ at inverse temperature $\beta=1/T$ and chemical potential μ is defined as

$$\mathcal{Z}(\beta,\mu)=\mathrm{tr}\left[\hat{P}\mathrm{e}^{-\beta(\mathcal{H}-\mu N)}\right] \tag{4}$$

where the trace is over both the $\mathbb{Z}_2$ gauge fields and the fermions. $\hat{P}=\prod_{\mathbf{r}}\hat{P}_{\mathbf{r}}$ is a projection operator, with $\hat{P}_{\mathbf{r}}$ enforcing the Gauss law constraint equation (3) at each site $\mathbf{r}$, and can be written as

$$\hat{P}_{\mathbf{r}}=\frac{1}{2}\left(1+\prod_{\boldsymbol{\eta}=\pm\hat{\mathbf{e}}_x,\hat{\mathbf{e}}_y}\sigma^x_{\mathbf{r}+\boldsymbol{\eta}}(-1)^{n_{\mathbf{r}}}\right) \tag{5}$$

In the path integral formulation, we will use an equivalent expression using a discrete Lagrange multiplier[1]

$$\hat{P}_r=\sum_{\lambda_{\mathbf{r}}=\pm1}\hat{P}_{\lambda_{\mathbf{r}}}=\frac{1}{2}\sum_{\lambda_{\mathbf{r}}=\pm1}\mathrm{e}^{i\frac{\pi}{2}(1-\lambda_{\mathbf{r}})\left(\sum_{\boldsymbol{\eta}}\frac{\left(1-\sigma^x_{\mathbf{r}+\boldsymbol{\eta}}\right)}{2}+n_{\mathbf{r}}\right)} \tag{6}$$

Following standard techniques, we use a Trotter decomposition to write the thermal density matrix as $\mathrm{e}^{-\beta\mathcal{H}}=\prod_{\tau=0}^{M-1}\mathrm{e}^{-\epsilon\mathcal{H}}$ with $\epsilon=\beta/M$ and introduce resolution of the identities in the σ^z basis, $\mathbb{1}=\sum_{\sigma^z}|\sigma^z\rangle\langle\sigma^z|$, between each imaginary time step. The matrix elements are then computed to order $\mathcal{O}(\epsilon^2)$. This results in an imaginary time path integral formulation of the partition that sums over spacetime configurations of the Ising gauge field. The Ising fields, $\lambda_{\mathbf{r}}$, are identified with the temporal gauge field in the Lagrangian formulation of the ILGT, and they are non-trivial only at the last time step (axial gauge).

The configuration Boltzmann weight, $W[\sigma^z_{r,\boldsymbol{\eta}},\lambda_{\mathbf{r}}]$, is a product of the Ising gauge field weight, $W_{\mathbb{Z}_2}[\sigma^z_{\mathbf{r},\boldsymbol{\eta}},\lambda_{\mathbf{r}}]$, and the fermions weight $W_{\mathrm{f}}[\sigma^z_{\mathbf{r},\boldsymbol{\eta}},\lambda_{\mathbf{r}}]$.

Explicitly, $W_{\mathbb{Z}_2}[\sigma^z_{\mathbf{r},\boldsymbol{\eta}},\lambda_{\mathbf{r}}]=\mathrm{e}^{-S\left[\sigma^z_{\mathbf{r},\boldsymbol{\eta}},\lambda_{\mathbf{r}}\right]}$, where the action, $S[\sigma^z_{\mathbf{r},\boldsymbol{\eta}},\lambda_{\mathbf{r}}]$, corresponds to the classical three-dimensional Ising gauge theory[1].

Tracing over the fermions for a given Ising gauge field configuration yields $W_{\mathrm{f}}[\sigma^z_{r,\boldsymbol{\eta}},\lambda_{\mathbf{r}}]=\prod_{\alpha=\uparrow,\downarrow}\det G^{-1}_{\alpha}[\sigma^z_{\mathbf{r},\boldsymbol{\eta}},\lambda_{\mathbf{r}}]$, where $G^{-1}_{\alpha}[\sigma^z_{\mathbf{r},\boldsymbol{\eta}},\lambda_{\mathbf{r}}]$ is the equal-time inverse fermion propagator at a fixed Ising gauge field configuration. We emphasize that the fermion weight depends explicitly on the temporal gauge fields.

The fermion determinant for each spin species, $W_{f,\alpha}$ is real because the gauge group is real and since the spin-up and spin-down weights are identical then the total weight $W_{\mathrm{f}}=W_{f,\uparrow}W_{f,\downarrow}=W^2_{f,\uparrow}>0$ is strictly non-negative. The QMC formulation is therefore free of the numerical sign problem. We note that the above discussion does not rely on the specific details of the lattice geometry, and therefore can be extended to other interesting lattice structures beyond the square lattice.

We sample the configuration space $\{\sigma^z_{\mathbf{r},\boldsymbol{\eta}},\lambda_{\mathbf{r}}\}$, using both a local single-spin update and global updating scheme based on the worm algorithm[48].

'Zero problem' at half-filling. At half-filling we faced an additional difficulty in our numerical simulation. In the Supplementary Methods, we show that, due to PH symmetry, all configurations satisfying $\prod_{\mathbf{r}}\lambda_{\mathbf{r}}=-1$ have vanishing fermionic weight, $W_{\mathrm{f}}=0$. As a consequence, these configurations are not sampled, giving rise to a systematic bias in computing observables that are not symmetric under PH transformation of a single-spin species.

To solve this problem, we used an extended configuration space that allows sampling of the missing weight. This approach may be of general interest for other QMC simulations. Finally, we benchmarked our numerical implementation against exact diagonalization on small lattices ($L=2$) and found excellent agreement within the error bars. Additional details on the QMC implementation can be found in the Supplementary Methods.

Observables. As a probe of the Ising gauge field sector we consider the average Ising magnetic flux energy $\langle B\rangle$ with

$$B=\sum_{\mathbf{r}}\prod_{b\in\square_{\mathbf{r}}}\sigma^z_b \tag{7}$$

and fluctuations are captured by Ising flux susceptibility,

$$\chi_{\mathrm{B}}=\frac{1}{N}\int_0^\beta \mathrm{d}\tau\left[\langle B(\tau)B(0)\rangle-\langle B(0)\rangle^2\right] \tag{8}$$

where N is the number of sites.

Superconducting order is probed by studying the s-wave pairing susceptibility, defined as

$$P_{\mathrm{SC}}\left(\mathbf{r}-\mathbf{r}',\tau\right)=\frac{1}{\sqrt{2}}\left\langle b^\dagger_{\mathbf{r}'}(\tau)b_{\mathbf{r}}+h.c\right\rangle \tag{9}$$

where $b^\dagger_{\mathbf{r}}=c^\dagger_{\mathbf{r},\downarrow}c^\dagger_{\mathbf{r},\uparrow}$ is the pair creation operator.

Charge density order is probed by studying the charge susceptibility, defined as

$$P_{\mathrm{D}}\left(\mathbf{r}-\mathbf{r}',\tau\right)=\left\langle n^{\mathrm{f}}_{\mathbf{r}'}(\tau)n^{\mathrm{f}}_{\mathbf{r}}\right\rangle \tag{10}$$

The s-wave pairing, Δ_{SC} and CDW, Δ_{CDW} order parameters are computed from their respective equal-time correlation functions

$$\Delta_{\mathrm{SC/CDW}}=\lim_{L\to\infty}\lim_{\beta\to\infty}\sqrt{P_{\mathrm{SC/CDWD}}(q=0/\{\pi,\pi\},\tau=0)/N} \tag{11}$$

and extrapolated first to zero temperature and then to the thermodynamic limit.

The current response to an external probe $U(1)$ electromagnetic gauge field is given by[49]

$$\Pi_{\mu,\nu}(\mathbf{q},i\omega_{\mathrm{m}})=\left\langle -K_\mu\right\rangle\delta_{\mu,\nu}-\left\langle J_\mu\left(\mathbf{q},i\omega_{\mathrm{m}}\right)J_\nu\left(-\mathbf{q},-i\omega_{\mathrm{m}}\right)\right\rangle \tag{12}$$

where the Matsubara frequency $\omega_{\mathrm{m}}=2\pi m/\beta$ with $m\in\mathbb{Z}$. The diamagnetic term is given by (minus) the fermion kinetic energy along the μ direction

$$K_\mu=-t\sum_{\mathbf{r},\alpha}\sigma^z_{\mathbf{r},\mu}c^\dagger_{\mathbf{r},\alpha}c_{\mathbf{r}+\mu,\alpha}+\mathrm{h.c.} \tag{13}$$

The current operator $J_{\mathbf{r},\mu}$ is defined as

$$J_{\mathbf{r},\mu}=-it\sum_{\mathbf{r},\alpha}\sigma^z_{\mathbf{r},\mu}c^\dagger_{\mathbf{r},\alpha}c_{\mathbf{r}+\mu,\alpha}-\mathrm{h.c.} \tag{14}$$

We are interested only in the static response here, which we decompose into its longitudinal (L) and transverse (T) parts

$$\Pi_{\mu,\nu}(\mathbf{q},i\omega_{\mathrm{m}}=0)=\Pi^{\mathrm{L}}(\mathbf{q})\frac{q_\mu q_\nu}{q^2}+\Pi^{\mathrm{T}}(\mathbf{q})\left(\delta_{\mu,\nu}-\frac{q_\mu q_\nu}{q^2}\right) \tag{15}$$

To characterize a superconducting state, we compute the superfluid stiffness $\rho_{\mathrm{s}}=\Pi^{\mathrm{T}}\left(\mathbf{q}\to0\right)$. In practice, on an $L\times L$ lattice, we compute[49]

$$\rho_{\mathrm{s}}=\lim_{L\to\infty}\Pi_{xx}\left(q_x=0,q_y=2\pi/L;i\omega_{\mathrm{m}}=0\right) \tag{16}$$

To characterize the deconfined Dirac phase, we use the static orbital (dia)magnetic susceptibility

$$\chi(\mathbf{q})=\frac{\partial M(\mathbf{q})}{\partial B(\mathbf{q})}=-\frac{1}{q^2}\Pi^{\mathrm{T}}\left(\mathbf{q}\right) \tag{17}$$

which can be related to $\partial M/\partial H$ using $B=H+4\pi M$. Note that this is the only place in the paper where we use B to denote the external magnetic field, related to $U(1)$ electromagnetism, and not the $\mathbb{Z}_2$ magnetic field!

Data availability. The data that support the plots within this paper and other findings of this study are available from the corresponding author upon reasonable request.

References

48. Prokof'ev, N. & Svistunov, B. Worm algorithms for classical statistical models. *Phys. Rev. Lett.* **87,** 160601 (2001).
49. Scalapino, D. J., White, S. R. & Zhang, S. Insulator, metal, or superconductor: the criteria. *Phys. Rev. B* **47,** 7995–8007 (1993).